Thin-Walled Structures 46 (2008) 1251–1261

Contents lists available at ScienceDirect

Thin-Walled Structures

journal homepage: www.elsevier.com/locate/tws

# Numerical and experimental investigations on buckling of steel cylindrical shells with elliptical cutout subject to axial compression

Mahmoud Shariati *, Masoud Mahdizadeh Rokhi

*Department of Mechanical Engineering, Shahrood University of Technology, Daneshgah Boulevard, Shahrood, Iran*

ARTICLE INFO

*Article history:*
Received 19 November 2007
Received in revised form
18 February 2008
Accepted 18 February 2008
Available online 10 April 2008

*Keywords:*
Buckling
Cylindrical shells
Elliptical cutout
Finite element analysis
Experimental method

ABSTRACT

The effect of cutouts on load-bearing capacity and buckling behavior of cylindrical shells is an essential consideration in their design.

In this paper, simulation and analysis of thin steel cylindrical shells of various lengths and diameters with elliptical cutouts have been studied using the finite element method and the effect of cutout position and the length-to-diameter ($L/D$) and diameter-to-thickness ($D/t$) ratios on the buckling and post-buckling behavior of cylindrical shells has been investigated. For several specimens, buckling test was performed using an INSTRON 8802 servo hydraulic machine and the results of experimental tests were compared to numerical results. A very good correlation was observed between numerical simulation and experimental results. Finally, based on the experimental and numerical results, formulas are presented for finding the buckling load of these structures.



## 1. Introduction

Cylindrical shells are frequently used in the manufacturing of aircrafts, missiles, boilers, pipelines, automobiles, and some submarine structures. These structures may experience axial compression loads in their longevity and yield to buckling. Furthermore, these structures usually have disruptions, such as cutouts, which may have adverse effects on their stability.

The problem of buckling in cylindrical shells has been a preoccupation of investigators for more than a century. At first, researchers focused on the determination of the buckling load in the linear elastic zone, but experimental studies [1,2] showed that the buckling capacity of thin cylindrical shells is much lower than the amount determined in the classic theories [3]. Based on the classic theories, the buckling load of thin cylindrical shells subject to uniform axial compression can be predicted using the formula

$$N_{cr} = \frac{E}{\sqrt{3(1-\nu^2)}}\left(\frac{t^2}{R}\right) \quad (1)$$

where $E$ is the Young modulus, $\nu$ is Poisson's ratio, $t$ is shell thickness, and $R$ is shell radius. It is noteworthy that this formula gives an appropriate result for thin shells without cutouts with $L/R \leqslant 5$ [4]. For shells with moderate thickness ($R/t < 50$), this formula often overestimates the buckling load, so that buckling occurs before reaching the specified load.

Van Dyke [5] determined the stress distribution around a hole in a cylindrical shell subject to axial, torsional, and internal pressure. Tennyson [6] performed an experimental study on the effect of circular cutouts on the buckling capacity of cylindrical shells with radius-to-thickness ratio of 162–331 subject to axial compression. He compared the measured buckling loads with analytical results of Van Dyke.

Brogan and Almorth [7] studied the effect of stiffened rectangular cutouts on the buckling load of cylindrical shells, and also compared the experimental results of shells with cutouts with and without stiffening with the results calculated by the STAGS finite element code. Jenkins [8] performed an experimental study on cylindrical shells in the range $75 \leqslant R/t \leqslant 150$ with two opposite circular cutouts. Additionally, Starnes [9] performed an experimental investigation on the buckling of cylindrical shells with circular cutout subject to axial compression. In this study, the radius-to-thickness ratio of shells was 400–960. Based on the findings from these experiments, he linearized the buckling problem and determined an upper bound for the buckling load using the Reyleigh–Ritz method.

Almorth and Holmes [10] investigated 11 thin-walled aluminum cylindrical shells with rectangular cutouts and various stiffeners which had been installed on seven test specimens. The buckling load of stiffened shells was compared to that of the non-stiffened specimens. Furthermore, the experimental results were compared with the results of the STAGS finite element code. Analysis results showed that the effects of stiffeners are negligible

* Corresponding author. Tel.: +98 273 3332230; fax: +98 273 3335600.
*E-mail addresses:* mshariati@shahroodut.ac.ir, mshariati44@gmail.com (M. Shariati).

0263-8231/$ - see front matter © 2008 Elsevier Ltd. All rights reserved.
doi:10.1016/j.tws.2008.02.005

for thin cylindrical shells with small cutouts, unless for long shells. Almorth et al. [11] performed a complex nonlinear analysis for cylindrical shells with two opposite circular cutouts subject to axial compression. They showed that the calculated numerical results are comparable to the experimental results of Starnes. Starnes [12] performed another experimental and numerical study on the buckling effect of circular, square, and rectangular cutouts in cylindrical shells subject to axial compression. Toda [13], too, performed an experimental investigation on the cylindrical shells with circular holes subject to axial compression. Furthermore, he placed ring-shaped stiffeners around the cutout and studied the effect of stiffeners on the buckling of cylindrical shells with circular cutouts. The shells in his study were made of polyester with two opposite circular cutouts, and they had a radius-to-thickness ratio of 100 and 400. It was found that if the holes were small enough, they had no effect on the buckling resistance of cylindrical shells. Larger holes, however, caused considerable decrease in the buckling load. Jullien and Limam [2] studied the effect of square, rectangular, and circular cutouts on the buckling of cylindrical shells subject to axial compression, and developed a parametrical formula for the shape and dimensions of the cutouts. The influences of the position and number of cutouts were also studied. The software program used for the finite element method was CASTEM2000. At the same time, Yeh et al. [14] analytically and experimentally studied the bending and buckling of moderately thick-walled cylindrical shells with cutouts. The dimensions of their shells were diameter-to-thickness, $D/t = 50$ and length-to-diameter, $L/D = 7.9$. It was found that the limiting buckling moment would be higher if the cutout was on the tension side rather than on the compression side. They also performed parametric studies on the influences of shape, size, and location of a cutout on the buckling capacity. Hilburger et al. [15] analyzed the buckling behavior of thin composite cylindrical panels with central circular cutout. In this study, the effect of cutout dimensions, panel curvature, and initial geometric imperfections was investigated, and the numerical results were compared with experimental findings. The STAGS finite element code was used for numerical analysis in this study. It was found that the results of nonlinear analyses are much more accurate than the traditional linear analyses. Tafreshi [16] also numerically studied the buckling and post-buckling response of composite cylindrical shells subjected to internal pressure and axial compression loads using ABAQUS. She studied the influences of size and orientation of cutouts and found that an increase of internal pressure resulted in an increase in buckling capacity. Haipeng Han et al. [17] studied the effect of dimension and position of square-shaped cutouts in thin and moderately thick-walled cylindrical shells of various lengths by nonlinear numerical methods using the ANSYS software. They also compared their results with experimental studies on moderately thick-walled shells. Finally, they developed several parametric relationships based on the analytical and experimental results using the least squares regression method.

In this paper, linear and nonlinear analyses using the ABAQUS finite element software, were carried out in order to study the effect of the position of elliptical cutouts with identical dimensions on the buckling and post-buckling behavior of cylindrical shells. The shells with different diameters and lengths as follows, studied were: $(L/D_1) = 2.857$, 6.5, 10; $(D_1/t) = 53.846$; and $(L/D_2) = 2.495$, 5.676, 8.732; $(D_2/t) = 61.667$. Additionally, several buckling tests were performed using an INSTRON 8802 servo hydraulic machine, and the results were compared with the results of the finite element method. A very good correlation between experiments and numerical simulations was observed. Finally, based on the experimental and numerical results, formulas are presented for the computation of the buckling load in such structures.

## 2. Numerical analysis using the finite element method

The numerical simulations were carried out using the general finite element program ABAQUS 6.4-PR11.

### 2.1. Geometry and mechanical properties of the shells

For this study, thin-walled cylindrical shells with three different lengths ($L = 120$, 273, 420 mm), and two different diameters ($D = 42$, 48.1 mm) were analyzed. An elliptical geometry was selected for cutouts that were created in the specimens. Furthermore, the thickness of shells was $t = 0.78$ mm. Fig. 1 shows the geometry of the elliptical cutouts. According to this figure, parameter ($a$) shows the size of the cutout along the longitudinal axis of the cylinder, and parameter ($b$) shows the size of the cutout in circumferential direction of the cylinder. The distance between the center of the cutout and the lower edge of the shell is designated by $L_0$, as shown in Fig. 1.

Specimens were nominated as follows: $D$42-$L$120-$L_0$60-$a$-$b$. The numbers following $D$ and $L$ show the diameter and length of the specimen, respectively.

The cylindrical shells used for this study were made of mild steel alloy. The mechanical properties of this steel alloy were determined according to ASTM E8 standard [18], using the INSTRON 8802 servo hydraulic machine.

The stress–strain curves, stress–plastic strain curve and respective values are shown in Fig. 2. Based on the linear portion of stress–strain curve, the value of elasticity module was computed as $E = 187.737$ GPa and the value of yield stress was obtained as $\sigma_y = 212$ MPa. Furthermore, the value of Poisson ratio was assumed to be $\nu = 0.33$.

### 2.2. Boundary conditions

For applying boundary conditions on the edges of the cylindrical shells, two rigid plates were used that were attached to the ends of the cylinder.

In order to analyze the buckling subject to axial load similar to what was done in the experiments; a 10-mm displacement was applied centrally to the center of the upper plate, which resulted in a distributed, compressive load on both edges of the cylinder. Additionally, all degrees of freedom in the lower plate and all degrees of freedom in the upper plate, except in the direction of longitudinal axis, were constrained.

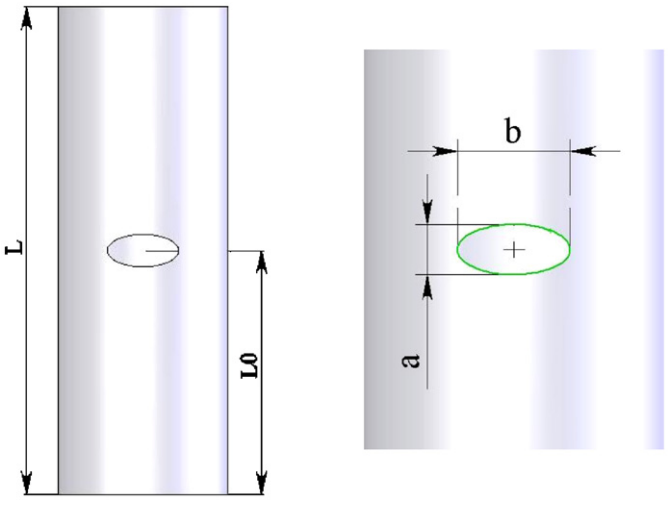


**Fig. 1.** Geometry of cutout.

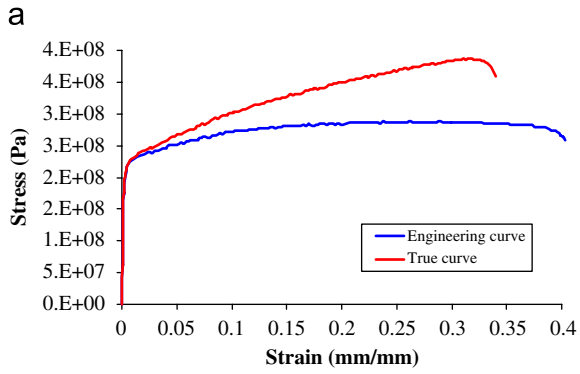


| True strain | True stress (MPa) |
|---|---|
| 0 | 0.000 |
| 6.58e-5 | 25.280 |
| 0.00023 | 63.010 |
| 0.00045 | 106.830 |
| 0.00066 | 150.620 |
| 0.00084 | 175.980 |
| 0.00104 | 191.07 |
| 0.00247 | 211.506 |
| 0.01225 | 235.136 |
| 0.02386 | 246.513 |
| 0.03496 | 254.419 |
| 0.04488 | 263.261 |
| 0.05622 | 271.512 |
| 0.06729 | 280.063 |
| 0.07536 | 284.217 |
| 0.08872 | 296.220 |
| 0.09999 | 301.781 |
| 0.11279 | 309.086 |
| 0.12660 | 316.361 |
| 0.13874 | 322.896 |
| 0.15396 | 328.374 |
| 0.16895 | 335.947 |
| 0.18456 | 343.195 |
| 0.19961 | 349.866 |
| 0.21384 | 355.697 |
| 0.22749 | 360.545 |
| 0.23999 | 365.326 |
| 0.25811 | 370.322 |
| 0.27509 | 377.857 |
| 0.29851 | 383.657 |
| 0.31556 | 387.465 |

| Plastic strain | True stress (MPa) |
|---|---|
| 0.00000 | 191.073 |
| 0.00135 | 211.506 |
| 0.00499 | 227.057 |
| 0.01431 | 239.110 |
| 0.02255 | 246.513 |
| 0.03360 | 254.419 |
| 0.04085 | 261.920 |
| 0.05478 | 271.512 |
| 0.06092 | 276.249 |
| 0.07385 | 284.217 |
| 0.08302 | 293.382 |
| 0.09838 | 301.780 |
| 0.10874 | 306.844 |
| 0.12052 | 314.189 |
| 0.13241 | 320.089 |
| 0.14318 | 325.627 |
| 0.15914 | 331.566 |
| 0.18551 | 345.820 |
| 0.19533 | 349.007 |
| 0.20636 | 354.279 |
| 0.21914 | 358.231 |
| 0.23106 | 362.571 |
| 0.24248 | 365.636 |
| 0.26052 | 372.000 |
| 0.27117 | 377.394 |
| 0.28148 | 378.330 |
| 0.29873 | 383.024 |
| 0.30904 | 386.024 |
| 0.31060 | 386.491 |
| 0.31208 | 387.571 |
| 0.31350 | 387.465 |

**Fig. 2.** (a) Stress–strain curves, (b) stress–plastic strain curve (for more information about true stress–strain curve and plastic property refer to [18], ABAQUS analysis user's manual, part IV, section 11.1.1). and respective values (over 150 data were obtained from tensile test; therefore some of them were shown here).

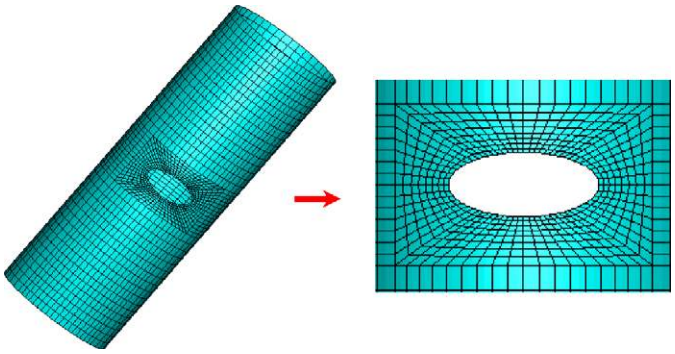

**Fig. 3.** A sample of FEM mesh.

In the section on experimental results, it will be shown that the fulcrum used in these tests has an edge that is 19.6 mm high. For this reason, in numerical simulations, the edges of the shell are constrained to this elevation except in the direction of cylinder axis.

### 2.3. Element formulation of the specimens

For this analysis, the nonlinear element S8R5, which is an eight-node element with six degrees of freedom per node, suitable for analysis of thin shells, and the linear element S4R, which is a four-node element were used [19]. Part of a meshed specimen is shown in Fig. 3. Both linear and nonlinear elements were used for the analysis of the shells, and the results were compared with each other.

### 2.4. Analytical process

Eigenvalue analysis overestimates the value of buckling load, because in this analysis the plastic properties of material do not have any role in analyses procedure. For buckling analysis, an eigenvalue analysis should be done initially for all specimens, to find the mode shapes and corresponding eigenvalues. Primary modes have smaller eigenvalues and buckling usually occurs in these mode shapes. For eigenvalues analysis the "Buckle" step was used in software. Three initial mode shapes and corresponding displacements of all specimens were obtained. The effects of these mode shapes must be considered in nonlinear buckling analysis (Static Riks step). Otherwise, the software would choose the buckling mode in an arbitrary manner, resulting in unrealistic results in nonlinear analyses. For "Buckle" step, the subspace solver method of the software was used.

It is noteworthy that due to the presence of contact constraints between rigid plates and the shell, the Lanczos solver method cannot be used for these specimens [19]. In Fig. 4, three primary mode shapes are shown for the specimen $D42$-$L120$-$L_0 60$-8-17.6.

After completion of the Buckle analysis, a nonlinear analysis was performed to plot the load–displacement curve. The maximum value in this curve is the buckling load. This step is called "Static Riks" and uses the arc length method for post-buckling analysis. In this analysis, nonlinearity of both material properties and geometry is taken into consideration.

### 2.5. Reference cylindrical shell

For plotting the curves, it is preferable to use dimensionless data. In this study, for making the buckling load dimensionless,

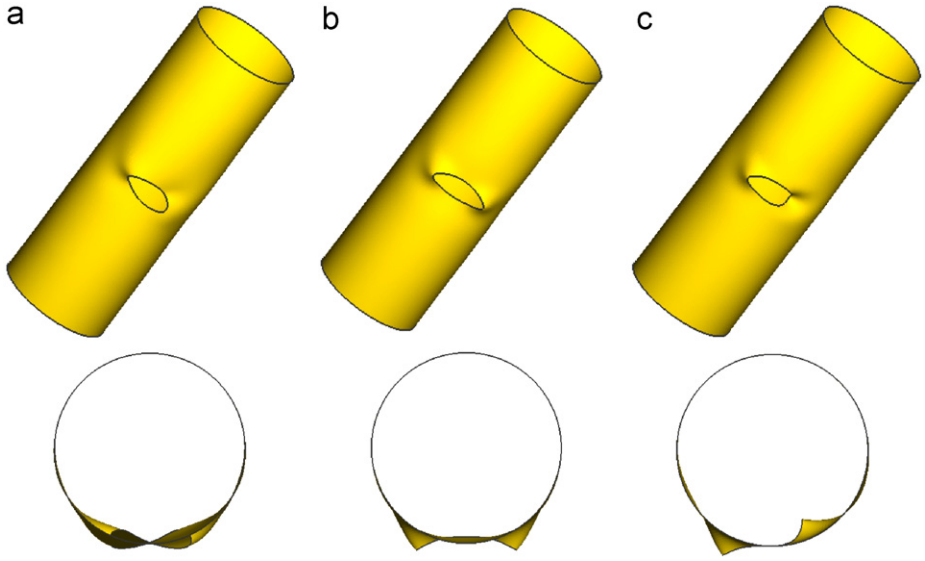


**Fig. 4.** Buckling mode shapes for specimen $D42$-$L120$-$L_0 60$-8-17.6: (a) first mode, (b) second mode, (c) third mode.

we used buckling of a reference cylindrical shell, which is defined as follows:

$$F_{\text{ref}} = \pi D t \times \sigma_y \tag{2}$$

where $F_{\text{ref}}$ is the reference load, which is in fact the load required for the cylindrical shell to yield. $D$ is the diameter, $t$ is the thickness of the shells, and $\sigma_y$ is the yield stress of the material used in the making of shells. Therefore, the reference load of the specimens is calculated in this way:

$$F_{\text{ref}} = \pi \times 42\,\text{mm} \times 0.78\,\text{mm} \times 212\,\text{N/mm}^2 = 21,818.738\,\text{N} \quad \text{for } D = 42\,\text{mm} \tag{3}$$

$$F_{\text{ref}} = \pi \times 48.1\,\text{mm} \times 0.78\,\text{mm} \times 212\,\text{N/mm}^2 = 24,987.65\text{N} \quad \text{for } D = 48.1\,\text{mm} \tag{4}$$

Also, the amount of compressive deformation of the shells was made dimensionless using the length of the shells.

## 3. Numerical analysis results

In this section, the results of the buckling analysis in cylindrical shells with elliptical cutouts of identical size in different positions using the finite element method were presented. For this purpose, a cutout with fixed dimensions was created on the shells with distances from the lower edge of the shell as $L_0 = 0.5L$, $0.6L$, $0.7L$, $0.8L$, and $0.9L$.

Three different shell lengths were analyzed, representing short, intermediate-length, and long/slender cylindrical shells. As mentioned previously, the boundary conditions are symmetric with reference to the mid-height of shells. Therefore, when the cutout is located along half of the shell length, due to the presence of symmetry, it would reflect the influence of the cutout's location along the entire length of the shells. For cylindrical shells, the results are obtained from nonlinear buckling analyses, including both geometric and material nonlinearity. The designation and analysis details of each model are summarized in Tables 1 and 2. Evidently, the results of this analysis can be generalized to shells with similar $L/D$ and $D/t$ ratios.

The results show that a change in the position of the cutout affects the buckling load. In Figs. 5 and 6, buckling load curves are plotted against the cutout position for cylindrical shells of various lengths for parameters $D/t = 53.846$ and 61.667, respectively.

It can be seen that an increase in the diameter of the shell increases the buckling load. Figs. 5 and 6 clearly show that with changing the position of the cutout from mid-height of the shell toward the edges, the buckling load increases. It can also be seen that longer shells are more sensitive to the change in the cutout position. For example, for shells with parameters $L/D = 10$ and $D/t = 53.846$, when the cutout position is changed from the middle of the shell to 90% of its length, the buckling load increases 11%, while for shells with parameters $L/D = 6.5$ and $D/t = 53.846$, the increase in the buckling load is only 8%, and for shells with parameters $L/D = 2.857$ and $D/t = 53.846$, the increase in the buckling load is limited to only 4%. Similarly, for shells with the ratio of $D/t = 61.667$, with the change of cutout position from middle to 90% of shell length, the buckling load changes 16%, 6%, and 3% for ratios $L/D = 8.732$, 5.676, and 2.495, respectively.

Fig. 7 shows the buckling load vs. the (L/D) ratio curves. It is clear that for fixed cutout position, buckling load decreases with the increase in the length of cylindrical shells, and shells with greater diameter have higher buckling loads.

### 3.1. Load vs. deformation curves

Figs. 8 and 9 show the load-end shortening curves, isometric and top views of the shells and von Mises stress contours for two specimens with ratios $L/D = 5.676$ and $D/t = 61.667$, with a cutout of fixed size in different positions ($L_0/L = 0.5$ and 0.7, respectively).

According to Figs. 8 and 9, it can be seen that before the load reaches a critical value, stress is uniformly distributed in all areas of the shell, except the regions around the cutout, and it increases with increasing load. In the specimen with a cutout in mid-height position, stress contours are totally symmetrical. The front region of the shell tolerates less stress because of the presence of the cutout (Figs. 8a and 9a), and the area of these regions increases with increase in load, until the load reaches the critical value. However, in regions around the cutout and in circumferential direction of the shell, stress rises briskly, so that these regions

**Table 1**
Summary of numerical analysis for cylindrical shells with Elliptical cutout

| $D = 42$ mm, $t = 0.78$ mm, $D/t = 53.846$ | | | | | |
|---|---|---|---|---|---|
| Model designation | Shell length (mm) | Cutout size ($a \times b$) (mm × mm) | Location of cutout ($L_0/L$) | Buckling load (N) | |
| | | | | S4R element | S8R5 element |
| *D42-L420-Perfect* | 420 | – | – | 23285.2 | 22792.8 |
| *D42-L420-*$L_0$210-8-17.7 | 420 | 8 × 17.7 | 0.5 | 17670.6 | 16938.7 |
| *D42-L420-*$L_0$252-8-18 | 420 | 8 × 18 | 0.6 | 17757.6 | 17020.5 |
| *D42-L420-*$L_0$294-8-18.15 | 420 | 8 × 18.15 | 0.7 | 18157.5 | 17453.2 |
| *D42-L420-*$L_0$336-8-18 | 420 | 8 × 18 | 0.8 | 18827 | 18185.6 |
| *D42-L420-*$L_0$378-8-18.04 | 420 | 8 × 18.04 | 0.9 | 19403.3 | 18729.1 |
| *D42-L273-Perfect* | 273 | – | – | 23447.4 | 22814.8 |
| *D42-L273-*$L_0$136.5-8-17.68 | 273 | 8 × 17.68 | 0.5 | 18477.7 | 17746.4 |
| *D42-L273-*$L_0$163.8-8-18 | 273 | 8 × 18 | 0.6 | 18527 | 17822.3 |
| *D42-L273-*$L_0$191.1-7.96-18.25 | 273 | 7.96 × 18.25 | 0.7 | 18888.5 | 18181.8 |
| *D42-L273-*$L_0$218.4-8-18 | 273 | 8 × 18 | 0.8 | 19153.7 | 18714.5 |
| *D42-L273-*$L_0$245.7-7.98-17.94 | 273 | 7.98 × 17.94 | 0.9 | 19698.5 | 19187.1 |
| *D42-L120-Perfect* | 120 | – | – | 23404.7 | 22751.6 |
| *D42-L120-*$L_0$60-8-17.6 | 120 | 8 × 17.6 | 0.5 | 19760.8 | 19120.4 |
| *D42-L120-*$L_0$72-8-17.6 | 120 | 8 × 17.6 | 0.6 | 19761 | 19174 |
| *D42-L120-*$L_0$84-8-17.6 | 120 | 8 × 17.6 | 0.7 | 19828.6 | 19338 |
| *D42-L120-*$L_0$108-8-17.6 | 120 | 8 × 17.6 | 0.9 | 20109.5 | 19891.4 |

**Table 2**
Summary of numerical analysis for cylindrical shells with elliptical cutout

| $D = 48.1$ mm, $t = 0.78$ mm, $D/t = 61.667$ | | | | | |
|---|---|---|---|---|---|
| Model designation | Shell length (mm) | Cutout size ($a \times b$) (mm × mm) | Location of cutout ($L_0/L$) | Buckling load (N) | |
| | | | | S4R element | S8R5 element |
| *D48.1-L420-Perfect* | 420 | – | – | 26506.4 | 25876.9 |
| *D48.1-L420-*$L_0$210-7.94-17.54 | 420 | 7.94 × 17.54 | 0.5 | 20592.8 | 19828.4 |
| *D48.1-L420-*$L_0$294-7.94-17.54 | 420 | 7.94 × 17.54 | 0.7 | 21237.1 | 20514.1 |
| *D48.1-L420-*$L_0$378-7.94-17.54 | 420 | 7.94 × 17.54 | 0.9 | 22502.5 | 21778.5 |
| *D48.1-L273-Perfect* | 273 | – | – | 26426.1 | 25858.7 |
| *D48.1-L273-*$L_0$136.5-8.02-17.86 | 273 | 8.02 × 17.86 | 0.5 | 21361.6 | 20623.2 |
| *D48.1-L273-*$L_0$191.1-8.02-17.86 | 273 | 8.02 × 17.86 | 0.7 | 21898.6 | 21192.3 |
| *D48.1-L273-*$L_0$245.7-8.02-17.86 | 273 | 8.02 × 17.86 | 0.9 | 22796.5 | 21872.9 |
| *D48.1-L120-Perfect* | 120 | – | – | 26484.7 | 25825.4 |
| *D48.1-L120-*$L_0$60−8.04-17.75 | 120 | 8.04 × 17.75 | 0.5 | 22827.5 | 22177.3 |
| *D48.1-L120-*$L_0$72-8-17.75 | 120 | 8 × 17.75 | 0.6 | 22830.1 | 22260.7 |
| *D48.1-L120-*$L_0$84-8-17.75 | 120 | 8 × 17.75 | 0.7 | 23006.9 | 22438.9 |
| *D48.1-L120-*$L_0$108-8-17.75 | 120 | 8 × 17.75 | 0.9 | 23734 | 22910.2 |

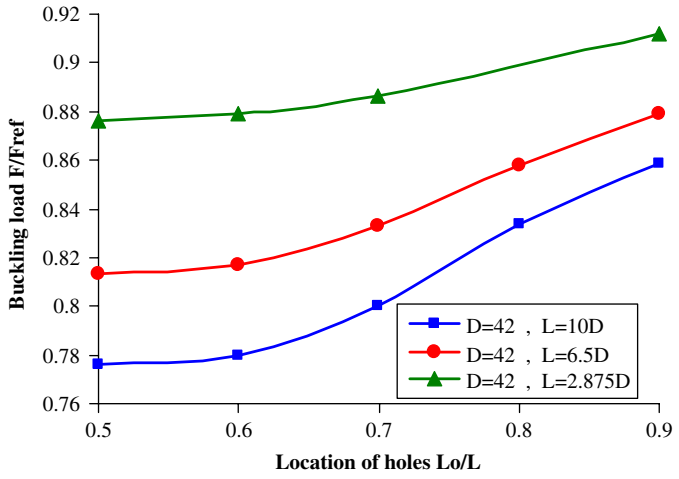


**Fig. 5.** Summary of the buckling capacity of cylindrical shells with ratio $D/t = 53.846$ and different lengths, with elliptical cutout situated at various locations.

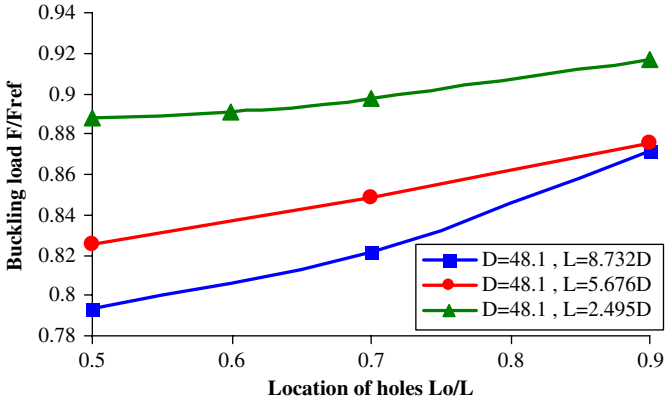


**Fig. 6.** Summary of the buckling capacity of cylindrical shells with ratio $D/t = 61.667$ and different lengths, with elliptical cutout situated at various locations.

yield before the shell reaches the buckling state (Figs. 8b and 9b). The area of these regions increases in circumferential direction with increase in load and finally the shell buckles.

Comparing Figs. 8 and 9, it can be deduced that with increasing $L_0/L$ ratio, stress distribution becomes more uniform before and after buckling, so that it approaches a uniform stress distribution in the shell, except for regions around the cutout. In other words, more regions of the shell experience the compression load. This can be the reason for the observation that buckling load increases with increase in $L_0/L$ ratio.

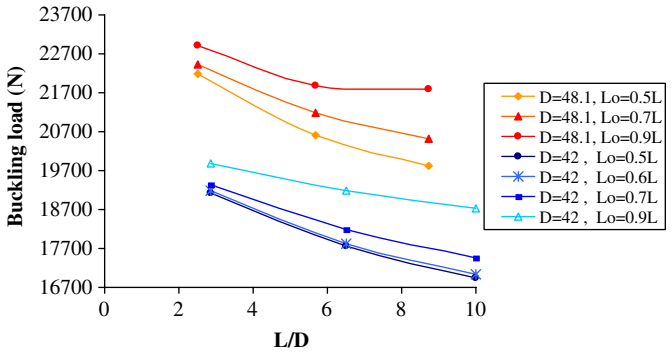


**Fig. 7.** Summary of the buckling capacity of cylindrical shells with different lengths and diameters, with elliptical cutout situated at various locations.

It can be seen that first the buckling occurs locally and then the shell experiences generalized bending. The FEM results also confirm this statement, since the obtained values for rotational displacements of the shell around an axis perpendicular to its longitudinal axis and parallel to the extension of the cutout along the circumferential direction of the shell for shells with ratios $L_0/L = 0.5$, 0.7, and 0.9 were 0.2, 0.15, and 0.1 rad, respectively, while for other regions, they were about 0.01, 0.009, and 0.006 rad, respectively.

Final load-end shortening curves for all analyzed specimens are shown in Figs. 10a–f. These curves are produced from finite element analyses with linear element S4R; because these elements have the post-buckling region better than other elements, according to the comparison done in Section 4 between numerical and experimental results.

It can be seen from these load-end shortening curves that the buckling load of the shell decreases considerably when a cutout is created in the shell. Furthermore, it can be seen that all curves related to shells with equal lengths have two coincidence points. The first coincidence point occurs just after the shells arrive at the buckling state. Before these points, the curves for shells with

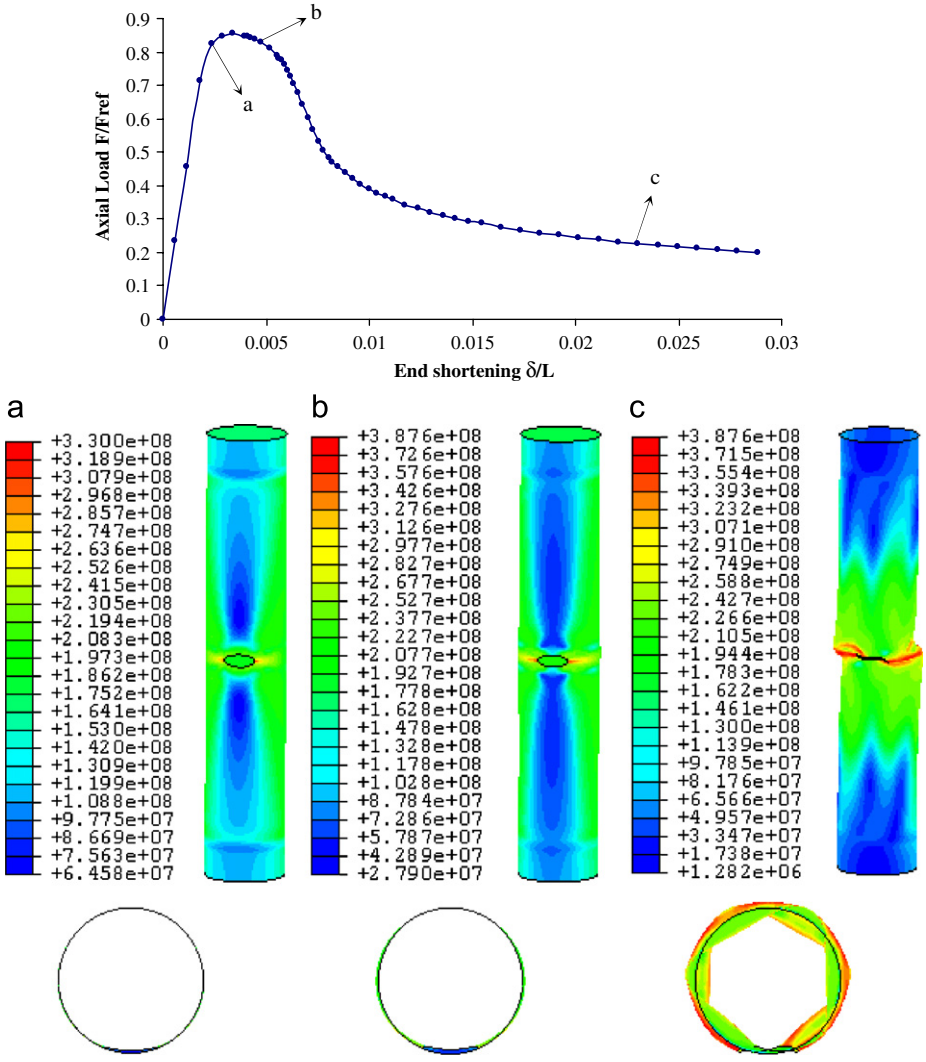


**Fig. 8.** Plots of load vs. end shortening, the shell deformations and the von Mises stress states at various loading stages of the specimen $D48.1$-$L273$-$L_0136.5$-8.02-17.86.

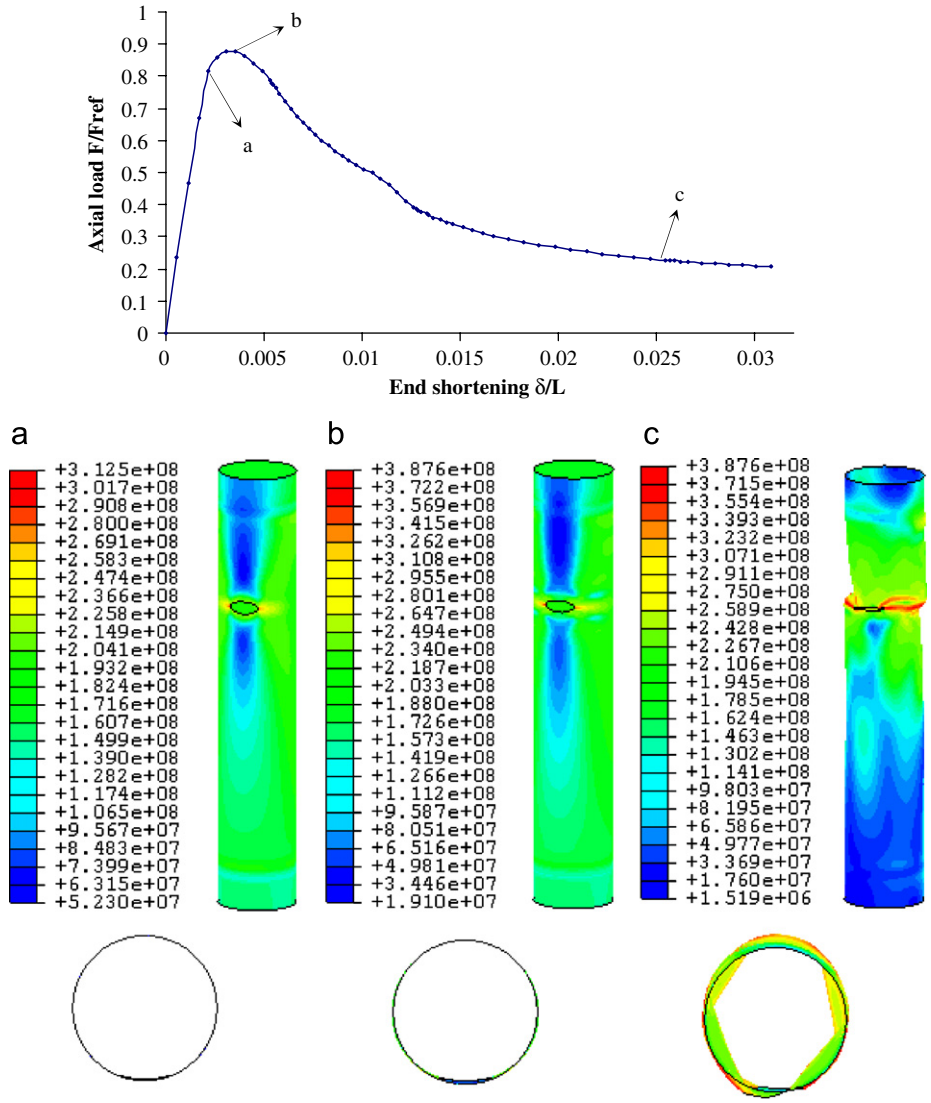


**Fig. 9.** Plots of load vs. end shortening, the shell deformations and the von Mises stress states at various loading stages of the specimen $D48.1$-$L273$-$L_0191.1$-8.02-17.86.

greater $L_0/L$ ratios are above other curve lines. This phenomenon happens once again for the second coincidence point, and the mutual position of curves reverses afterwards.

The reason behind this phenomenon is because of the resulting load redistribution. A high level of load redistribution results in a high load bearing capacity and vice versa [17].

Another observation is that with decreasing length of the specimens, the first coincidence point moves toward the buckling point. The equality of the slope of the curves in the pre-buckling region is another fact resulting from scrutinizing the charts.

## 4. Confirmation of numerical results with experimental findings

Experimental tests were performed on a large number of specimens in order to confirm the numerical results. For these tests, a state-of-the-art, servo hydraulic, INSTRON 8802 machine was used.

The specimens were constrained by steel sleeve fixtures inserted at both ends, which mimics the fixed–fixed boundary condition used in the finite element simulations (see Fig. 11). Three specimens were tested for each case and almost identical results were obtained compared to those obtained from the numerical simulations.

The results of experiments are compared with numerical findings in Table 3. It is evident that there is little difference between experimental and numerical results. For example, the biggest discrepancy between the two sets of results is 6.54% for S8R5 nonlinear element and 5.4% for S4R linear element. It is also noteworthy that the greatest difference is seen for short specimens. This can be attributed to the fact that the bending theory of shells is more suitable for lower $t/L$ ratios, and this theory is used by the software for calculations.

The mean difference between the numerical calculations and the experimental results is 2.89% for S4R element and 2.05% for S8R5 element. It can be said that the results of analysis with nonlinear elements have lower errors.

The load–displacement curves produced by numerical and experimental analyses are shown in Figs. 11–13 for three specimens. After comparing the curves in Fig. 11, it can be said that linear elements in comparison to nonlinear elements, have a

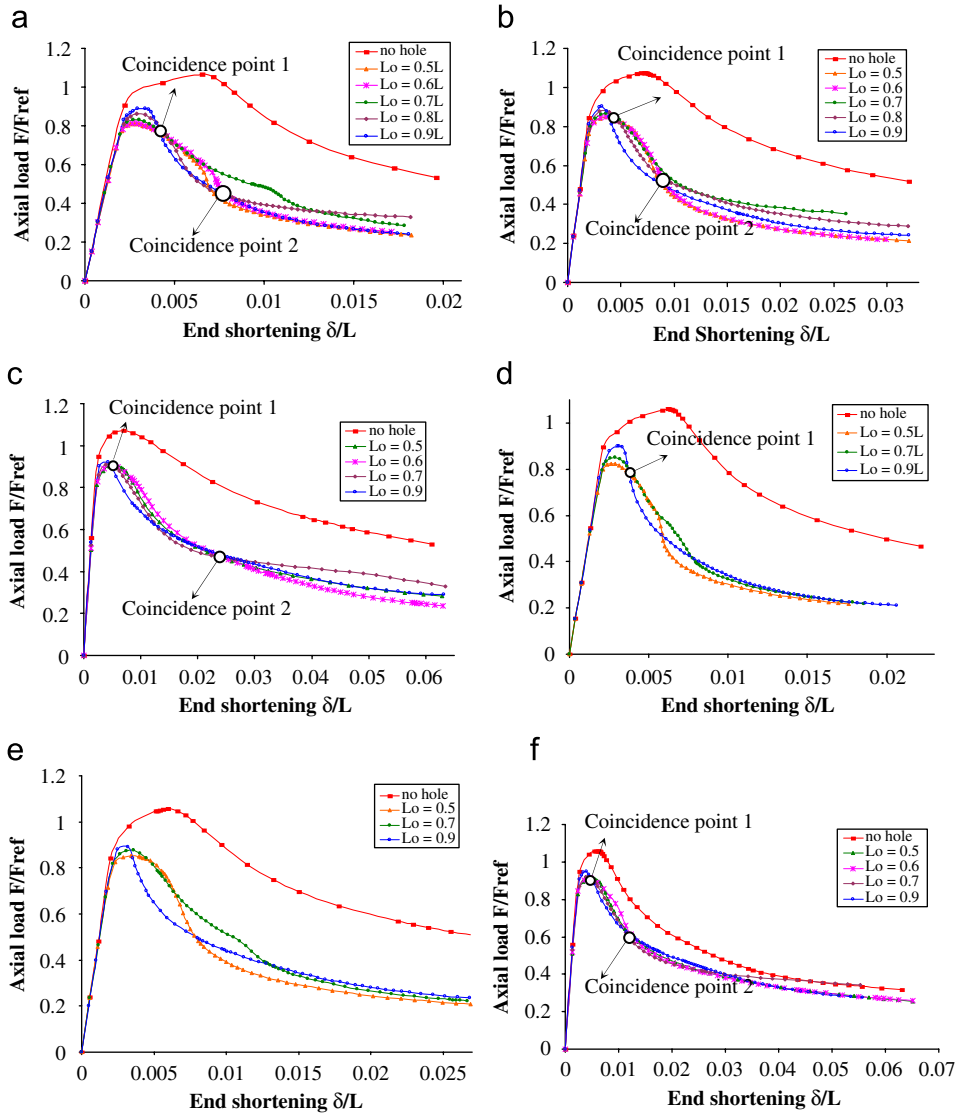


**Fig. 10.** Load-end shortening behavior of cylindrical shells with and without an elliptical cutout at various positions: (a) $L/D = 10$ and $D/t = 53.846$, (b) $L/D = 6.5$ and $D/t = 53.846$, (c) $L/D = 2.857$ and $D/t = 53.846$, (d) $L/D = 8.732$ and $D/t = 61.667$, (e) $L/D = 5.676$ and $D/t = 61.667$, (f) $L/D = 2.495$ and $D/t = 61.667$.

**Table 3**
Comparison of the experimental and numerical results for cylindrical shells with elliptical cutout situated at various locations

| Model designation | Buckling load (N) | | | $\lvert F_{EXP}-F_{FEM}\rvert/F_{EXP} \times 100\%$ error | |
|---|---|---|---|---|---|
| | S4R element | S8R5 element | Experimental | S4R element | S8R5 element |
| *D42-L420-Perfect* | 23285.2 | 22792.8 | 23018.3 | 1.16 | 0.98 |
| *D42-L420-*$L_0$210-8-17.7 | 17670.6 | 16938.7 | 16809.8 | 5.12 | 0.77 |
| *D42-L420-*$L_0$294-8-18.15 | 18157.5 | 17453.2 | 18555.2 | 2.14 | 5.93 |
| *D42-L420-*$L_0$378-8-18.04 | 19403.3 | 18729.1 | 19525 | 0.62 | 4.07 |
| *D42-L273-Perfect* | 23447.4 | 22814.8 | 22245.6 | 5.4 | 2.56 |
| *D42-L273-*$L_0$136.5-8-17.68 | 18477.7 | 17746.4 | 17945.8 | 2.96 | 1.11 |
| *D42-L273-*$L_0$191.1-7.96-18.25 | 18888.5 | 18181.8 | 17979.1 | 5.06 | 1.13 |
| *D42-L273-*$L_0$245.7-7.98-17.94 | 19698.5 | 19187.1 | 19296.2 | 2.08 | 0.56 |
| *D42-L120-Perfect* | 23404.7 | 22751.6 | 23925.7 | 2.17 | 4.90 |
| *D42-L120-*$L_0$60-8-17.6 | 19764.8 | 19120.4 | 20274.9 | 2.51 | 5.69 |
| *D42-L120-*$L_0$84-8-17.6 | 19828.6 | 19338 | 20691.3 | 4.16 | 6.54 |
| *D48.1-L420-Perfect* | 26506.4 | 25876.9 | 25775.3 | 2.84 | 0.39 |
| *D48.1-L420-*$L_0$210-7.94-17.54 | 20592.8 | 19828.4 | 19909.4 | 3.43 | 0.40 |
| *D48.1-L273-Perfect* | 26426.1 | 25858.7 | 26123.8 | 1.16 | 1.01 |
| *D48.1-L273-*$L_0$136.5-8.02-17.86 | 21361.6 | 20623.2 | 20855.3 | 2.43 | 1.11 |
| *D48.1-L120-Perfect* | 26484.7 | 25825.4 | 26967.3 | 1.79 | 4.23 |
| *D48.1-L120-*$L_0$60-8.04-17.75 | 22827.5 | 22177.3 | 21914 | 4.17 | 1.2 |

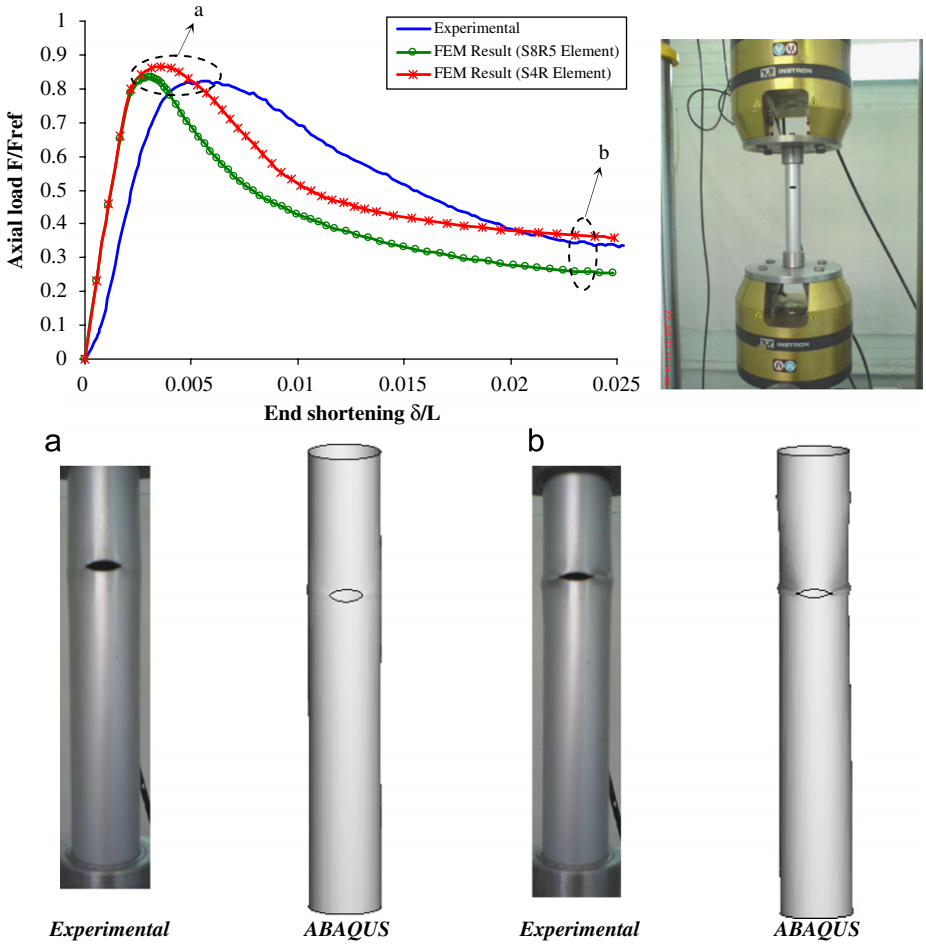


**Fig. 11.** Comparison of the experimental and numerical results for the specimen $D42$-$L273$-$L_0191.1$-7.96-18.25.

better prediction power for the post-buckling behavior of mild steel alloy cylindrical shells with elliptical cutouts. In the pre-buckling phase, both elements produce similar results.

It can be seen that the slope of load vs. end shortening curves is higher in numerical results than in experimental results before the buckling. This discrepancy is due to the presence of internal defects in the material which reduces the stiffness of the specimens in the experimental method, while the materials are assumed to be ideal in the numerical analyses.

## 5. Empirical–numerical equations

Based on the numerical and experimental dimensionless buckling loads of shells, formulas are presented here using Lagrangian polynomial for the computation of the buckling load of cylindrical shells with elliptical cutouts subject to axial compression. To get these formulas with using Lagrangian polynomial method [20], the surfaces were passed through the dimensionless buckling load values in ($K_{cutout}$, $\gamma$, $\lambda$) coordinate system which $K_{cutout}$ is buckling load reduction factor for cylindrical shells with cutout (dimensionless buckling load), $\gamma = L/D$ and $\lambda = L_0/L$.

$K_{cutout}$ is defined as follows:

$$K_{cutout} = \frac{F_{cutout}}{F_{perfect}} \tag{5}$$

where $F_{perfect}$ is the buckling load for cylindrical shells without cutouts and $F_{cutout}$ is the buckling load for cylindrical shells with cutouts. The general form of $K_{cutout}$ is as follows:

$$K_{cutout}(\gamma,\lambda) = A + B\gamma + C\gamma^2 + D\lambda + E\lambda^2 + F\gamma\lambda + \cdots \tag{6}$$

The coefficients $A$, $B$, $C$,... are computed using Lagrangian polynomial. To use these expressions, the buckling load for cylindrical shells without cutout must be known.

The formulas for computation of the buckling load of cylindrical shells with elliptical cutouts will be presented later in this paper. These relationships were formulated using experimental findings, and in a few cases where experimental data were not available, the numerical results with the S8R5 element were used:

$$K_{cutout} = 0.548\gamma - 3.517\lambda^2 - 0.0447\gamma^2 - 0.62 - 0.097\gamma^2\lambda^2 + 0.1353\gamma^2\lambda + 1.288\gamma\lambda^2 - 1.735\gamma\lambda + 4.702\lambda \tag{7}$$

$$K_{cutout} = 0.4171\lambda + 0.6544 - 0.00333\gamma^2 - 0.00138\gamma^2\lambda^2 + 0.00608\gamma^2\lambda + 0.0708\gamma^2\lambda - 0.1314\gamma\lambda + 0.0487\gamma - 0.1928\lambda^2 \tag{8}$$

Eq. (7) represents the reduction factor applicable to the cylindrical shells with the ratio $D/t = 53.846$ and various lengths ($2.857 \leqslant L/D \leqslant 10$), with an elliptical cutout of fixed size $8 \times 18\,\text{mm}^2$ in different positions.

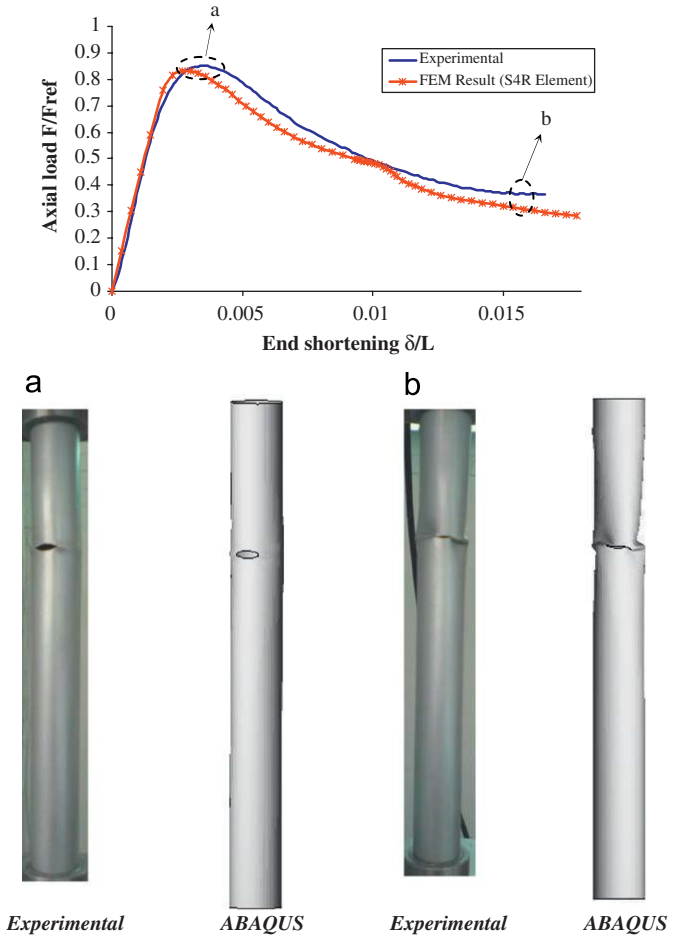


**Fig. 12.** Comparison of the experimental and numerical results for the specimen *D*42-*L*420-$L_0$294-8-18.15.

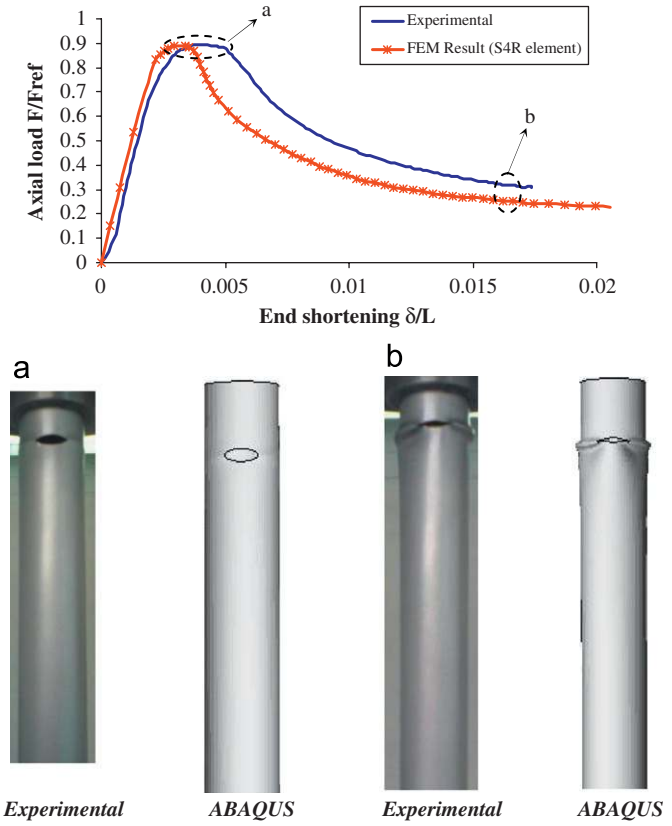


**Fig. 13.** Comparison of the experimental and numerical results for the specimen *D*42-*L*420-$L_0$378-8-18.04.

Eq. (8) represents the reduction factor applicable to the cylindrical shells with the ratio $D/t = 61.667$ and various lengths ($2.4948 \leqslant L/D \leqslant 8.732$), with an elliptical cutout of fixed size $8 \times 18\,\text{mm}^2$ in different positions.

## 6. Concluding remarks

In this research, we studied the buckling load of mild steel cylindrical shells of various $D/t$ and $L/D$ ratios with elliptical cutouts using numerical and experimental methodology, and determined the buckling load of these shells with a cutout of fixed size in different positions. The following results were found in this study:

Changing the position of the cutout from the mid-height of the shell toward the edges increases the buckling load, and longer shells are more sensitive to the change in cutout position.

Increasing the shell diameter with a fixed thickness increased the buckling load. And an increase in the $L/D$ ratio reduces the buckling load.

For cylindrical shells with cutout, at first the buckling occurs locally, and then the shell experiences general bending.

Comparison of the curves shows that the numerical and experimental results are well matched. Furthermore, the curves from linear elements predict the post-buckling region better than nonlinear elements, while the nonlinear elements are a better indicator of the buckling load.

Finally, we obtained formulas for computing the buckling load of shells with cutout based on the buckling load of perfect shells. These expressions can be used for a vast range of thin cylindrical shells with elliptical cutouts.

## References

[1] Arbocz J, Hol JMAM. Collapse of axially compressed cylindrical shells with random imperfections. AIAA J 1991;29:2247–56.
[2] Jullien JF, Limam A. Effect of openings on the buckling of cylindrical shells subjected to axial compression. Thin Wall Struct 1998;31:187–202.
[3] Timoshenko SP, Gere JM. Theory of elastic stability. 2nd ed. New York: McGraw-Hill; 1961.
[4] Ugural AC. Stresses in plates and shells. New York: McGraw-Hill; 1981.
[5] Van Dyke P. Stresses about a circular hole in a cylindrical shells. AIAA J 1965;33(9):1733–42.
[6] Tennyson RC. The effects of unreinforced circular cutouts on the buckling of circular cylindrical shells under axial compression. J Eng For Industry, ASME 1968;90:541–6.
[7] Brogan FA, Almorth BO. Buckling of cylindrical shells with cutouts. AIAA J 1970;8(2):236–40.
[8] Jenkins WC. Buckling of cylinders with cutouts under combined loading. MDAC paper WD 1390, McDonnel-Douglas Astronautics Co., Western Division, 1970.
[9] Starnes JH, Jr. The effect of a circular hole on the buckling of cylindrical shells. PhD thesis, California Institute of Technology, 1970.
[10] Almorth BO, Holmes AMC. Buckling of shells with cutouts, experiment and analysis. Int J Solids Struct 1972;8:1057–71.
[11] Almorth BO, Brogan FA, Marlowe MB. Stability analysis of cylinders with circular cutouts. AIAA J 1973;11(11):1582–4.
[12] Starnes Jr. JH. The effects of cutouts on the buckling of thin shells. In: Fung YC, Sechler EE, editors. Thin-shell structures. Englewood Cliffs, NJ: Prentice-Hall; 1974. p. 289–304.
[13] Toda S. Buckling of cylinders with cutouts under axial compression. Exp Mech 1983;23(4):414–7.

[14] Yeh MK, Lin MC, Wu WT. Bending buckling of an elastoplastic cylindrical shell with a cutout. Eng Struct 1999;21:996–1005.
[15] Hilburger MW, Vicki OB, Michael PN. Buckling behavior of compression-loaded quasi-isotropic curved panels with a circular cutout. Int J Solids Struct 2001;38:1495–522.
[16] Tafreshi A. Buckling and postbuckling analysis of composite cylindrical shells with cutout subjected to internal pressure and axial compression load. Int J Pressure Vesssel Piping 2002;79:351–9.
[17] Haipeng Han, Cheng J, Taheri F, Pegg N. Numerical and experimental investigations of the response of aluminum cylinders with a cutout subject to axial compression. Thin-Walled Struct 2006;44:254–70.
[18] ASTM A370-05, Standard test methods and definitions for mechanical testing of steel products.
[19] ABAQUS 6.4 PR11 user's manual.
[20] Gerald CF, Wheatley PO. Applied numerical analysis. New York: Addison-Wesley; 1999.